

Polarization Calibration and Imaging: Hercules A EVLA Data

DRAFT W. D. Cotton, April 11, 2013

Abstract—This memo describes the calibration and imaging of the linear polarization data from the EVLA demo observations of Hercules A. The calibration technique is outlined and its limitations detailed. Modifications to the wide band imaging technique needed to accommodate linear polarization are described. Overall results are satisfactory except at X band where clear artifacts from the instrumental polarization calibration remain.

Index Terms—interferometry, polarization, calibration

I. INTRODUCTION

POLARIMETRIC observations at radio wavelengths provide a great deal of information about the magnetic fields in, and the media in front of, radio sources. Radio interferometric polarimetry requires the determination and removal of the spurious instrumental polarized response. This memo discusses the methods applied to the calibration and imaging of the EVLA science demonstration observations of the radio galaxy Hercules A. Some preliminary results are presented. The techniques described in this memo are implemented in the Obit package [1]¹.

II. WIDE-BAND POLARIZATION CALIBRATION

Phase sensitive detectors such as used in heterodyne receivers like those in the EVLA are sensitive only to a single polarization state. In order to measure the full polarization state of the incoming waves, two detectors measuring orthogonal polarizations are needed. In an interferometer, all four cross correlations of the two pairs of detectors are made. These correlations can then be transformed into those for the Stokes parameters for imaging. In practice, the polarization state measured by the detectors (AKA “feeds”) is not precisely the desired state. This imperfection, if uncorrected, will lead to a spurious polarized response which is termed “instrumental polarization”. Correction of instrumental polarization for the EVLA is discussed in detail in [2] and [3].

Another calibration needed for arrays like the EVLA which detect right- and left-hand circular polarizations is the phase and delay offsets between the two polarization systems. The standard delay and phase calibration allows for an offset between the two systems; these offsets need to be determined and removed. The effect of a Right-Left phase offset is to rotate the apparent angle of the polarization vector on the sky. This calibration is referred to as “polarization angle calibration” or “Right-Left phase calibration”. Polarization angle calibration is discussed in [4] and [5].

National Radio Astronomy Observatory, 520 Edgemont Rd., Charlottesville, VA, 22903 USA email: bcotton@nrao.edu

¹<http://www.cv.nrao.edu/~bcotton/Obit.html>

A. Instrumental Polarization Calibration

The traditional technique [2] for determining unknown instrumental polarization parameters using a calibrator(s) with unknown polarization is to use the different effect of parallactic angle on the source and instrumental components of the cross polarized signal. One of the major difficulties with polarimetric calibration with the EVLA is that the instrumental polarization may be large and varies considerably with frequency. On the other hand, the polarization of a typical QSO calibrator is a few percent and varies only slowly with frequency. The traditional approach of a joint solution does not work well when the solutions are on many, relatively narrow band, low SNR data. A two stage approach to this calibration is adopted and described in the following.

The calibration provided by the Obit standard EVLA calibration scripts [6] allows for the traditional polarization including determining instrumental and calibrator polarizations, the Right-Left delay calibration and a Right-Left phase bandpass calibration. The first does not require a calibration of known polarization but the latter two require that a calibrator of known polarization angle be used. This standard calibration is initially applied to the data.

A subsequent stage, using functions in Obit module EVLAPolnScripts.py images the instrumental polarization calibrators and determines the fractional linear polarization and the polarization angle. A subsequent calibration (Obit/PCal) fixes the calibrator polarization and solves only for the instrumental polarization in blocks of channels. After the instrumental terms are recomputed and applied, the Right-Left delay and Right-Left phase bandpass are redetermined.

B. Polarization Angle Calibration

The Right-Left delay and phase bandpasses are determined using Obit/RLDly and Obit/RLPass respectively. These are done multiple times, the first in the standard calibration after the initial calculation of the instrumental polarization and then again after the final instrumental polarization calibration.

III. WIDE-BAND POLARIZATION IMAGING

Wide-band imaging in Obit/MFImage [7] is accomplished by dividing the observed total bandpass into frequency bins which are narrow enough that the bandwidth does not cause significant problems. A frequency variable taper and/or Briggs Robustness factor is used to adjust the resolution in each frequency bin to approximately the same. Deconvolution using CLEAN proceeds by forming a combined image which is used to select pixels at which CLEAN components are determined

and each CLEAN component records the value at the given pixel in each of the frequency bins. The combined image is CLEANed using the combined beam and the images in each frequency bin are CLEANed using the dirty beam from that frequency bin. When the CLEAN is complete, each frequency bin is restored using the components subtracted from it and a spectrum is fitted in each pixel. In the following, the modifications to the technique of [7] needed for improved imaging linear polarization are described. The following is implemented in Obit class ObitImageMF in function Combine.

For continuum total intensity (Stokes I) imaging, the source spectrum and instrumental effects change slowly enough with frequency that relatively coarse frequency bins (e.g. 5%) can be used. Faraday rotation of linear polarization may cause fairly rapid rotation in the Q-U plane with frequency producing rapid variations of the derived images in Stokes Q and U. The frequency bins used for Q and U imaging need to be narrow enough that bandwidth depolarization caused by averaging over too much frequency is negligible.

The combined dirty/residual image used to select CLEAN component pixel is the RMS weighted average of the individual bins. Represent each i of n frequency bin images, \mathbf{P}_i , as a vector of pixels. The weighted average of these is then

$$\mathbf{P} = \frac{1}{\sum_{i=0}^n \sigma_i} \sum_{i=0}^n \mathbf{P}_i \sigma_i$$

where σ_i is the standard deviation of the pixel values in \mathbf{P}_i derived from a histogram analysis.

This scheme is reasonable when all elements of \mathbf{P}_i are estimates of the same value. It is possible that a given element in \mathbf{P} averages to zero when some of the corresponding elements of the \mathbf{P}_i differ from zero. This may be especially the case for linear polarization Stokes Q or U images where Faraday rotation across the bandpass can rotate data in the Q-U plane. This rotation by itself may average the given Q or U value in a pixel to zero causing that pixel to be ignored in the CLEAN. It is common in pixels with significant Faraday rotation for the pixel value in \mathbf{P} to approach zero while the values in the \mathbf{P}_i are still far from zero.

In the case of non zero elements in \mathbf{P}_i averaging to zero, a modification to \mathbf{P} is needed. The function of \mathbf{P} is to guide the location at which CLEAN components are located and does not otherwise affect the final image and within limits may be modified.

An additional component can be added to \mathbf{P} to form \mathbf{P}' which causes pixels in which significant nonzero values in the \mathbf{P}_i have averaged to zero in \mathbf{P} instead to have values causing them to be included in the selection of locations of CLEAN components. This allows the residuals in the \mathbf{P}_i to approach zero. The original implementation of Obit/MFImage included such a modification to \mathbf{P} which proved inadequate for some cases of Stokes Q and U and the following describe a strengthening of this modification.

Consider a set of pixel values based on the maximum extrema of the residuals in

$$\mathbf{R}_i = \mathbf{P}_i - \mathbf{P}$$

. The extrema (largest deviation from zero) over i expressed in units of the RMS about zero in \mathbf{R}_i is

$$\mathbf{E} = \text{extrema}(R_i, s, \sigma 0_{R_i}).$$

In each element of the residual image, the *extrema* function picks the maximum in i of the element in $R_i / \sigma 0_{R_i}$ more deviant from zero than $s \sigma 0_{R_i}$. This selects the most significant extrema among the residual images in each element leaving zeroes where there is no significant deviation. The value of s used is 5. The extrema are then converted into equivalent flux density units in the frequency bin with the lowest RMS residuals by

$$\mathbf{E}' = \min(\sigma 0_{R_i}) \mathbf{E}$$

\mathbf{E}' could be added to \mathbf{P} which would cause the pixels with high residuals among the i to be CLEANed. However, the elements of \mathbf{E}' were selected on a pixel by pixel basis in a highly nonlinear fashion; this results in a function which is not a convolution with the dirty beam. This will cause major instabilities in CLEAN possibly resulting in an arbitrary number of components digging holes and filling them in.

This difficulty can largely be avoided by convolving \mathbf{E}' with the dirty beam before adding it to \mathbf{P}

$$\mathbf{P}' = \mathbf{P} + \frac{\lambda}{\text{beam_area}} (\mathbf{E}' \star \mathbf{B}).$$

where \star denotes convolution and \mathbf{B} is the elements of the combined dirty beam. The units of the $\mathbf{E}' \star \mathbf{B}$ are normalized to flux densities by dividing by the beam area of the dirty beam and the factor λ attenuates the effect of the extrema on \mathbf{P}' . A value of 0.1 is used for λ for Stokes I and 0.25 for Stokes Q and U.

Finally, a choice between using \mathbf{P} or \mathbf{P}' in the CLEAN is made on the basis of the most significant element of $R_i / \sigma 0_{R_i}$. \mathbf{P}' is used iff

$$\max(|\mathbf{P}|) < \frac{\max(|\mathbf{E}|)}{\sqrt{(n)}}$$

and

$$\max(|\mathbf{E}|) > t \min(\sigma 0_{R_i})$$

where the value of t for imaging Stokes I is 10 and for Stokes Q and U, 5.

The final fitted wide-band Stokes Q or U image is only meaningful in pixels in which the fractional Q or U is constant across the bandpass. In other cases, a Faraday analysis with frequency using the individual frequency bins is needed.

IV. EXAMPLE: HERCULES A

The radio galaxy Hercules A (3C348) was observed as an EVLA science demonstration project (TDEM0011) using the L (1-2 GHz), S (2-4 GHz), C (4-8 GHz) and X (8-9 GHz) band receivers. C and X band observations were made in all four configurations and L and S band in C, B and A configurations. The array was incompletely outfitted with S band receivers and the configuration was suboptimal for imaging and these data have not been processed. The bulk of the antennas during these observations used the old, narrow band X band systems. The 8 bit samplers were used for these observations giving a total

instantaneous bandwidth of 2 GHz; the C band observations were divided into two frequency settings covering the lower and upper halves of the 4 GHz bandpass available. These are referred to in the following as Clo and Chi. The observations are summarized in Table I.

Observations included 3C286 as the primary photometric calibrator which was also used for bandpass and Right-Left delay and phase bandpass calibration. J1651+0129 was used as the primary astrometric calibrator and at the higher frequencies the instrumental polarization calibrator. J1504+1029 was used as a secondary instrumental polarization calibrator. 3C48 was included as a backup photometric and bandpass calibrator. All these calibrators were used in the Delay calibration.

The observations were processed in a number of stages.

- 1) Standard calibration and editing
This uses the procedures described in [6].
- 2) Second pass instrumental polarization calibration
The fractional polarizations and polarization angles derived from the initial calibration were used to derive the instrumental polarization of blocks of 5 MHz at L band and 10 MHz at the higher frequencies. The values used are described in Table II. This table gives the fitted fractional polarizations and R-L phases (except for 3C286) used in the instrumental polarization calibration.
- 3) Self calibration of Hercules A
Herc A data were self calibrated using a CLEAN model derived in each band at each configuration. In A and B configurations, the several datasets were combined to generate the calibration model.
- 4) Refinement of amplitude calibration
Calibration models for 3C286 were derived for the various bands and forced to the standard spectrum of [8]. This model was used to derive correction to the amplitude calibration and then applied to Herc A.
- 5) Self calibration of combined Herc A datasets.
The various observations of Herc A in each band were combined using Obit/UVAppend which applied the prior calibrations, including polarization calibration. These data were then jointly self-calibrated using the Obit

TABLE I
Hercules A Observations

Config	Date	session	dur.(h)	L	S	Clo	Chi	X
D	2010-09-02	Da	3			X ¹	X	X
C	2010-12-17	Ca	8	X		X	X	X
B	2011-03-01	Ba	6.5	X		X	X	X
B	2011-03-07	Bb	9	X			X	X
B	2011-03-27	Bc	4.5	X		X	X	X
A	2011-08-28	Aa	8	X				
A	2011-08-03	Ab	8	X				
A	2011-09-03	Ac	8			X	X	X
A	2011-09-10	Ad	8			X	X	X
A	2011-09-06	Ae	1.5					
A	2011-09-06	Af	1.5			X	X	X

¹ an X indicates that useful data were obtained.

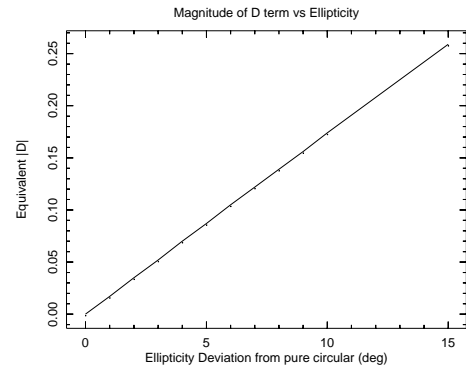


Fig. 10. Equivalence between the deviation of ellipticity from pure circular and the magnitude of the “D term”[9].

wide-band imager MFImage in one or two iterations of phase self cal. The imaging frequency bins were the sub-bands (IFs) of the observations.

- 6) Imaging of Herc A data
The self-calibrated data sets were imaged in Stokes I,Q and U using a multi-resolution CLEAN in MFImage. The fractional bandpass of the frequency bins was set to 2%.
- 7) Combination of bands
The various band images were aligned on the central core, convolved to a common set of resolutions and interpolated to a common grid. A low resolution set of images using 1.5” Gaussians was used to include the L band data and a high resolution of 0.45” for only the higher frequencies. The various datasets were then combined into MFImage style cubes in I, Q and U. Planes badly affected by data loss due to the RFI editing were omitted on the basis of a visual inspection. Combined spectra and rotation measure images were derived from pixel-by-pixel fitting.

A. Instrumental Polarization Calibration

If the instrumental polarization is stable, then the accuracy of its determination can be evaluated from the consistency of the fitted values in time and frequency. The derived values of the instrumental polarization terms for selected antennas are shown in Figures 1 – 9. In order to avoid contamination by RFI, only the higher frequencies and data from the A and B configurations are shown. The equivalence in the deviation of ellipticity from pure circular and the magnitude of the D terms are given in Figure 10.

Figures 1 – 9 indicate an instrumental polarization of typically a few percent with some spectacular deviations (see Fig. 8). The fitted values are generally stable in time and smoothly varying in frequency, again with the exception of Antenna 14 X band. Note: when feeds are close to circular, the orientation becomes poorly defined and this becomes evident in these figures. There appears to be more consistency in frequency that in time suggesting that the instrumental terms are not completely stable. However, the nonlinear solutions in Obit/PCal are initialized in the first block of channels in a sub-band (IF) and the final solution in one block is used as the

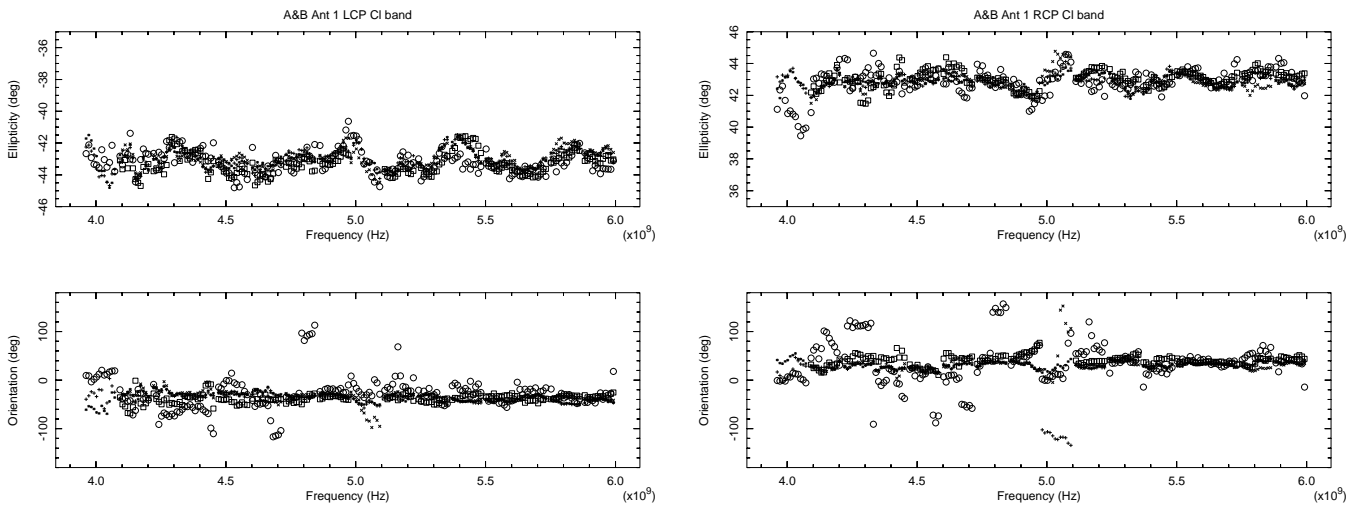


Fig. 1. Fitted instrumental polarization from A and B configuration as feed ellipticity and orientation Antenna 1 Clo band. LCP on left and RCP on right, ellipticities of $+45^\circ$ and -45° are pure right- and left-hand. + = A config 2011-09-03, * = A config 2011-09-10, open circle = A config 2011-09-06, x = B config 2011-03-01, open square = B config 2011-03-27.

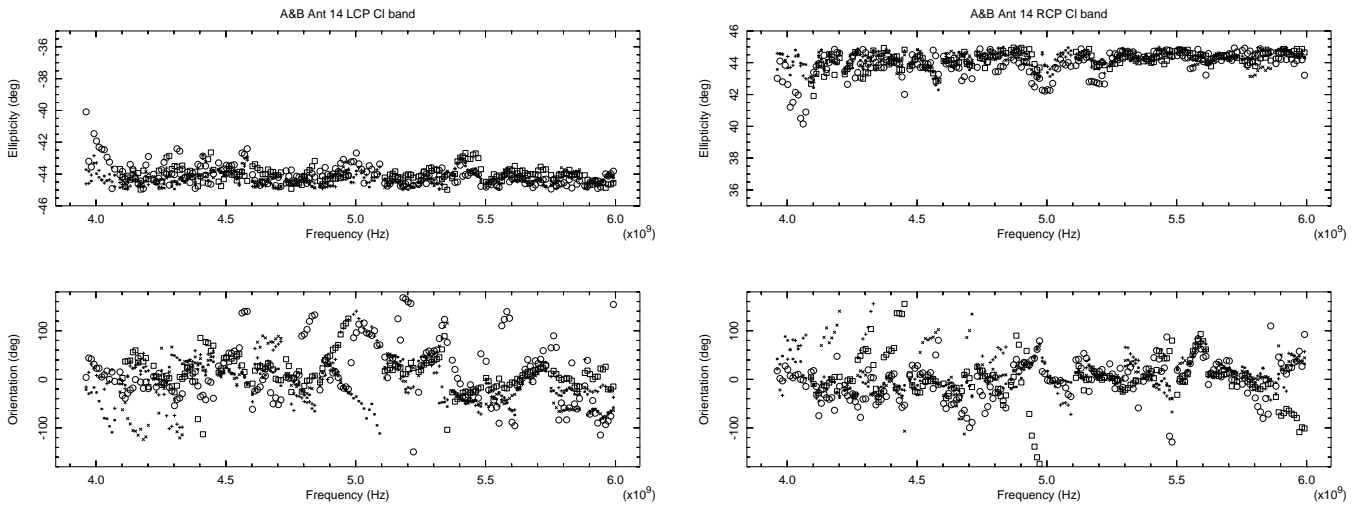


Fig. 2. Like Figure 1 except for antenna 14.

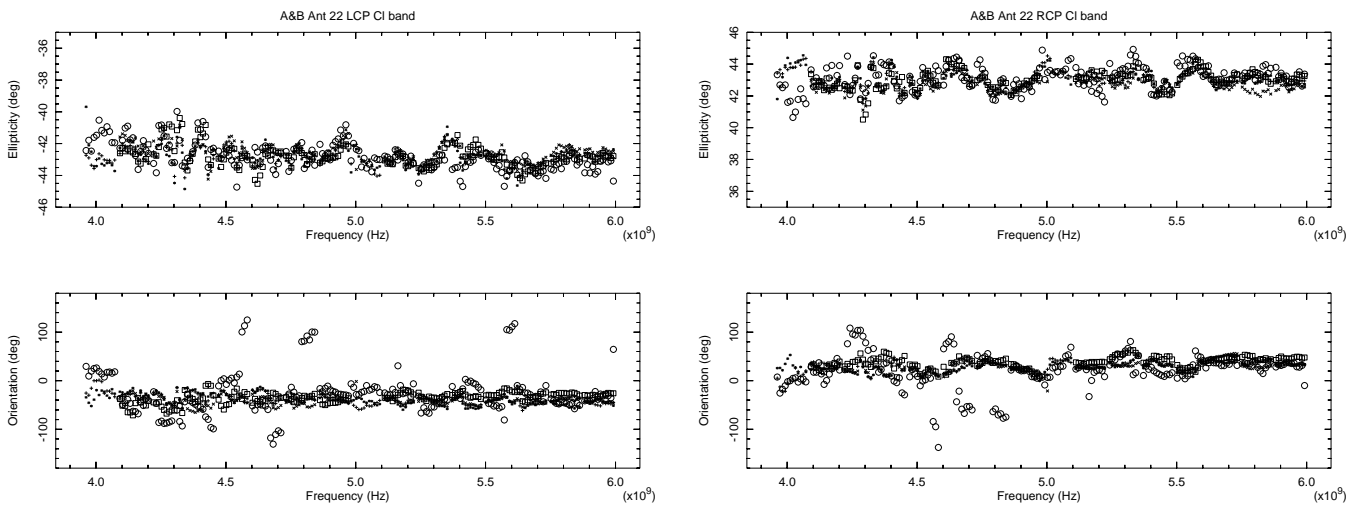


Fig. 3. Like Figure 1 except for antenna 22.

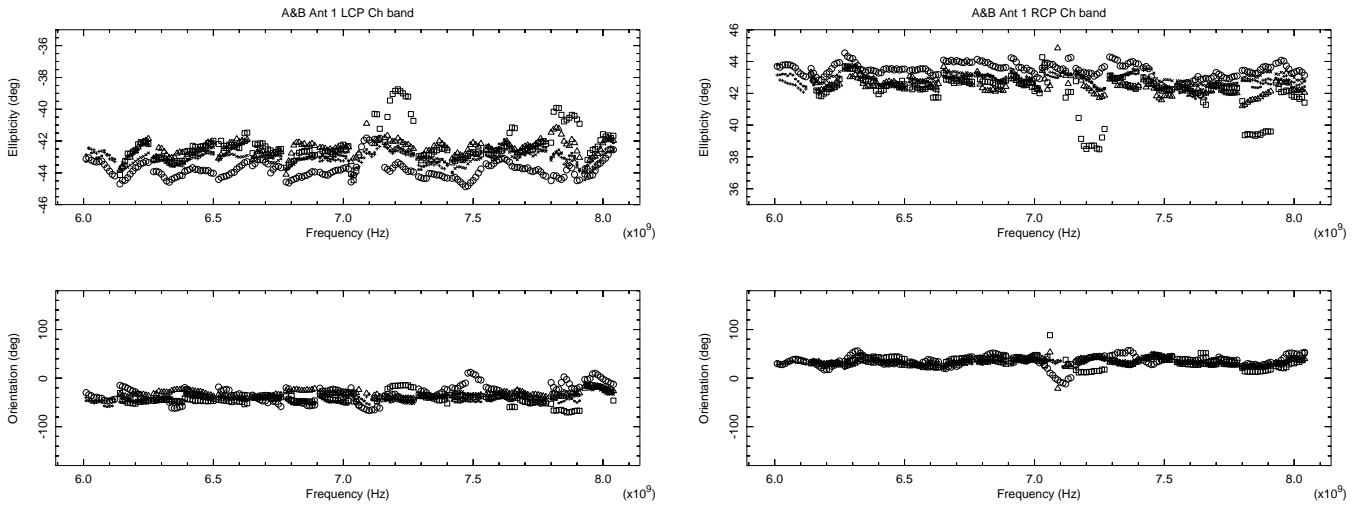


Fig. 4. Fitted instrumental polarization from A and B configuration as feed ellipticity and orientation Antenna 1 Chi band. LCP on left and RCP on right, ellipticities of +45° and -45° are pure right- and left-hand. + = A config 2011-09-03, * = A config 2011-09-10, open circle = A config 2011-09-06, x = B config 2011-03-01, open square = B config 2011-03-07, open triangle = B config 2011-03-27.

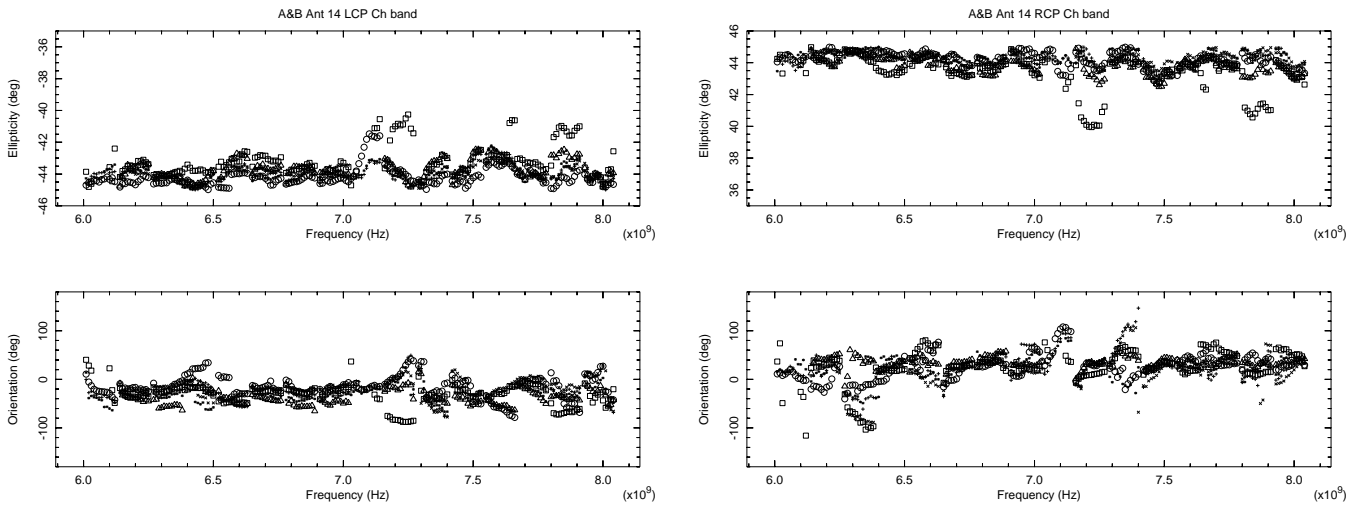


Fig. 5. Like Figure 4 except for antenna 14.

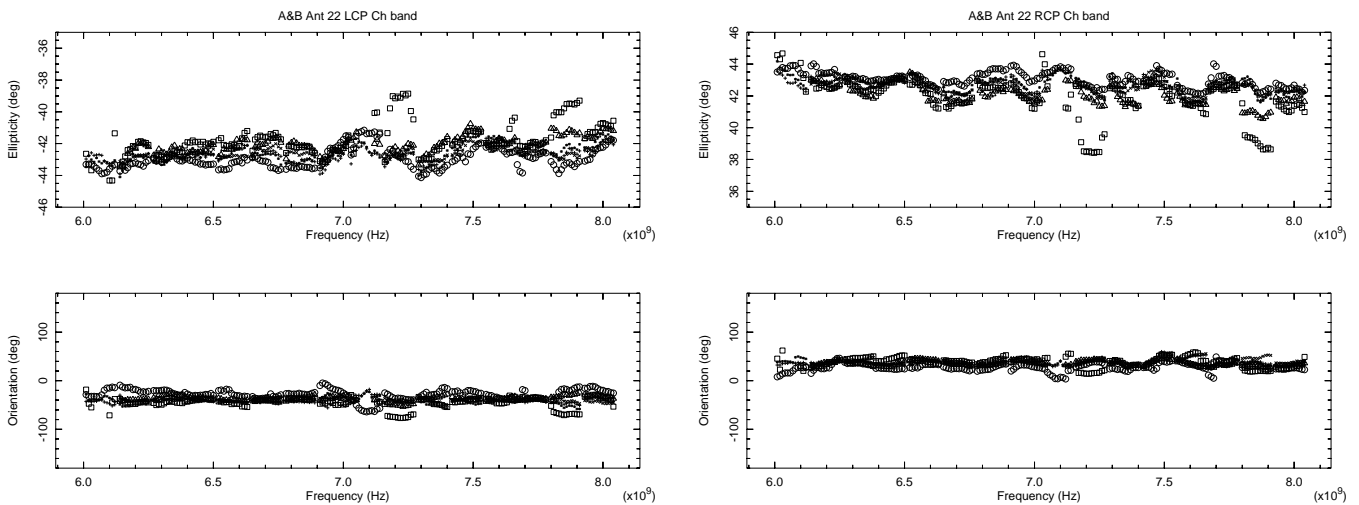


Fig. 6. Like Figure 4 except for antenna 22.

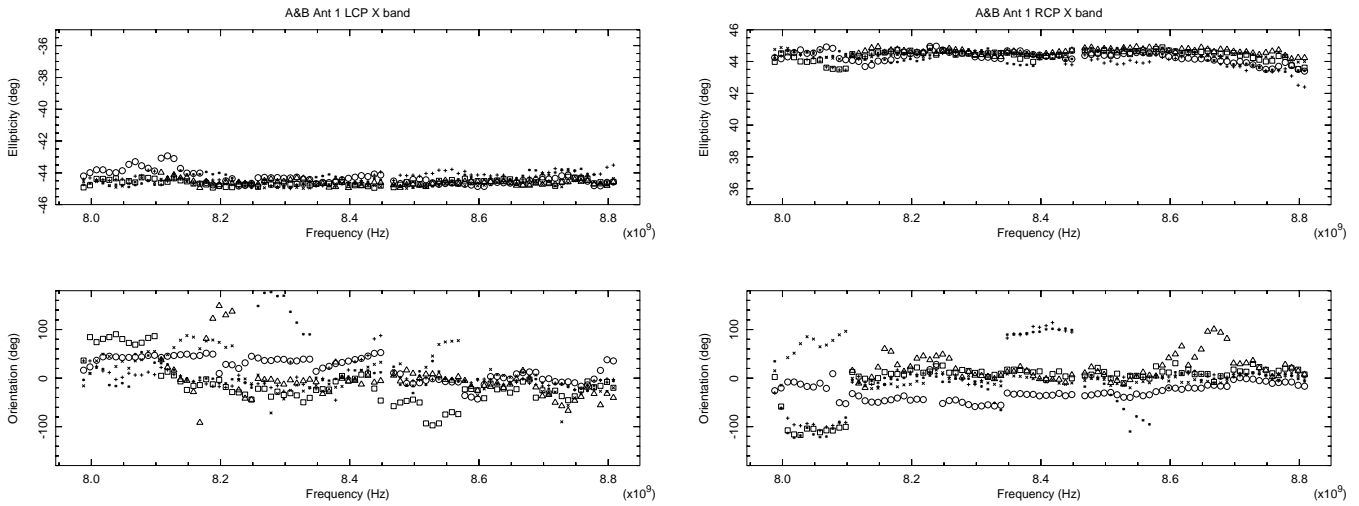


Fig. 7. Fitted instrumental polarization from A and B configuration as feed ellipticity and orientation Antenna 1 X band. LCP on left and RCP on right, ellipticities of $+45^\circ$ and -45° are pure right- and left-hand. + = A config 2011-09-03, * = A config 2011-09-10, open circle = A config 2011-09-06, x = B config 2011-03-01, open square = B config 2011-03-07, open triangle = B config 2011-03-27.

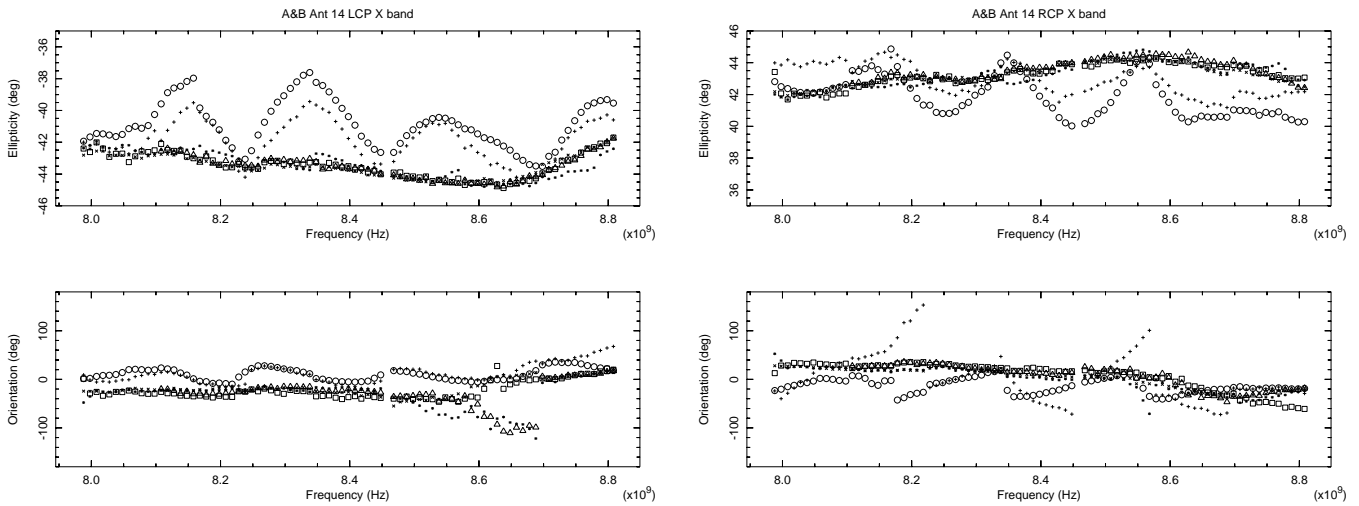


Fig. 8. Like Figure 7 except for antenna 14.

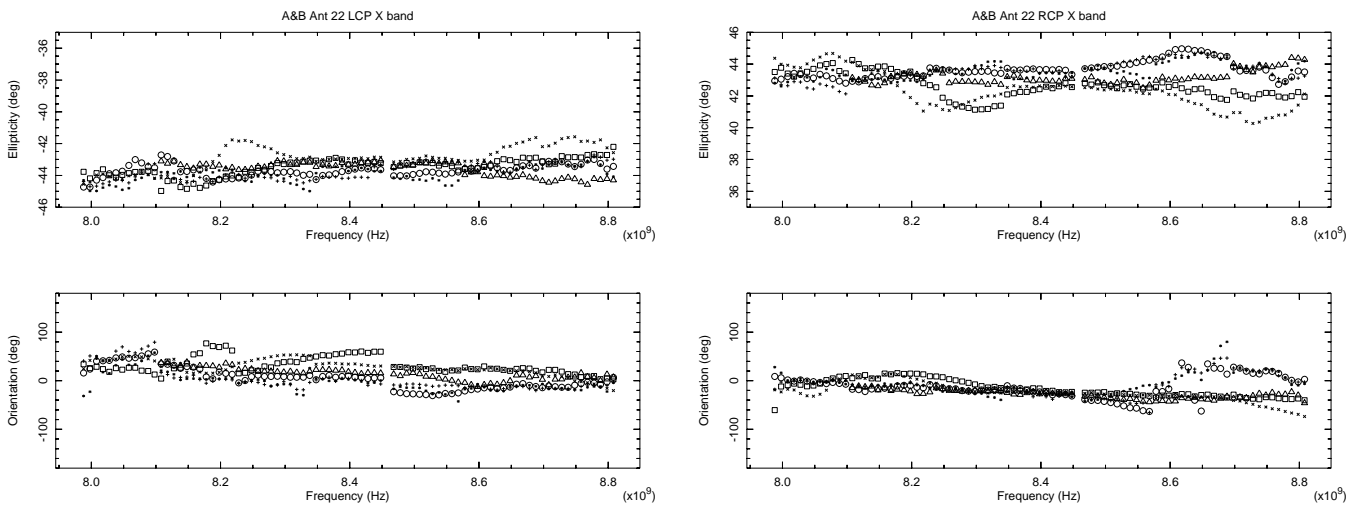


Fig. 9. Like Figure 7 except for antenna 22.

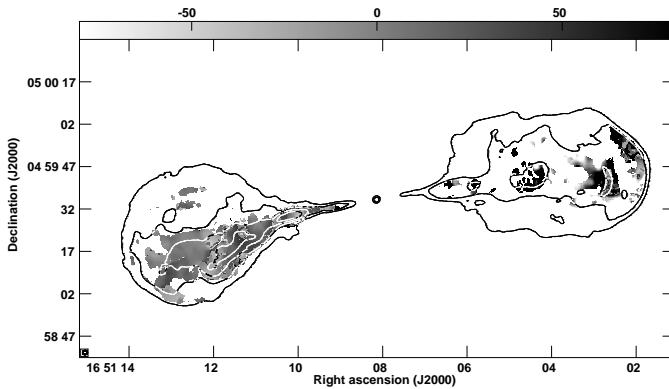


Fig. 13. Hercules A Low resolution (0.45'') combined 1-9 GHz images. Rotation measure in gray-scale with scale bar at top in rad/m^2 ; Stokes I in contours at -5, 5, 15, 50 and 150 mJy/bm .

starting solution in the subsequent block. This introduces both continuity inside a sub-band and sometimes discontinuities between sub-bands. This tendency can be seen in most of the plots and suggests that the parameters are not very well constrained by the data.

B. Imaging Stokes Q and U

The wide-band imaging used by the Obit task MFImage was intended for Stokes I in which the image changes slowly with frequency. However, the same technique works for Stokes Q and U, especially with the modification described in Section III. The L band data is most sensitive to the effects of Faraday rotation as it has the largest range of wavelength²; the planes imaged in Stokes Q are shown in Figure 11. This figure shows considerable changes across the band including sign changes; this is especially visible where the jet becomes visible in the upper right corner.

The quality of the polarization calibration appears to vary with frequency with the X band (8-9 GHz) appearing the worst. A comparison of the averaged Stokes Q polarization between Chi band (6-8 GHz) and X band (8-9 GHz) is given in Figure 12. Instrumental polarization calibration errors are generally manifested as apparently polarized artifacts away from regions of emission. Such artifacts are clearly visible in Figure 12 lower. Removing antennas with very large instrumental polarizations resulted in no visible improvement.

C. Image and Rotation Measure Analysis

Stokes I images and high reliability rotation measure images of the combined, low and high resolution of Herc A are shown in Figures 13 – 15. The derivation of the rotation measure images were such that artifacts in the X band portion of the overall spectrum were suppressed.

V. DISCUSSION

This memo outlines a method of calibration and imaging wide-band EVLA data which produces usable results. EVLA science demonstration data on the radio galaxy Hercules A is calibrated, imaged and rotation measure images derived. An iterative instrumental polarization calibration is used to

improve the stability of the narrow band intervals over which these terms were derived. An enhancement of the wide-band imaging used in Obit/MFImage allows better convergence in the CLEAN. Over most of the frequency range covered there appear to be few noticeable polarization calibration artifacts; however, at X band systematic artifacts appears. The reason for this is not understood

REFERENCES

- [1] W. D. Cotton, "Obit: A Development Environment for Astronomical Algorithms," *PASP*, vol. 120, pp. 439-448, 2008.
- [2] W. D. Cotton, "On-axis Instrumental Polarization Calibration for Circular Feeds," *Obit Development Memo Series*, vol. 30, pp. 1-13, 2012. [Online]. Available: <ftp://ftp.cv.nrao.edu/NRAO-staff/bcotton/Obit/PCalRL.pdf>
- [3] —, "On the Stability of EVLA C Band Polarization," *Obit Development Memo Series*, vol. 31, pp. 1-10, 2012. [Online]. Available: <ftp://ftp.cv.nrao.edu/NRAO-staff/bcotton/Obit/EVLACPoln.pdf>
- [4] —, "A New Method for Cross Polarized Delay Calibration of Radio Interferometers," *Obit Development Memo Series*, vol. 28, pp. 1-5, 2012. [Online]. Available: <ftp://ftp.cv.nrao.edu/NRAO-staff/bcotton/Obit/RLDly.pdf>
- [5] W. D. Cotton, "a New Method for Cross Polarized Delay Calibration of Radio Interferometers," *Journal of Astronomical Instrumentation*, vol. 1, p. 50001, Dec. 2012.
- [6] W. D. Cotton, "EVLA Continuum Scripts: Outline of Data Reduction and Heuristics," *Obit Development Memo Series*, vol. 29, pp. 1-25, 2012. [Online]. Available: <ftp://ftp.cv.nrao.edu/NRAO-staff/bcotton/Obit/EVLAObitScripts.pdf>
- [7] —, "High dynamic range wide bandwidth imaging," *Obit Development Memo Series*, vol. 19, pp. 1-9, 2010. [Online]. Available: <ftp://ftp.cv.nrao.edu/NRAO-staff/bcotton/Obit/MFImage.pdf>
- [8] R. A. Perley and B. J. Butler, "An Accurate Flux Density Scale from 1 to 50 GHz," *Ap. J. Suppl.*, vol. 204, p. 19, Feb. 2013.
- [9] A. R. Thompson, J. M. Moran, and G. W. Swenson, Jr., *Interferometry and Synthesis in Radio Astronomy, 2nd Edition*, Thompson, A. R., Moran, J. M., & Swenson, G. W., Jr., Ed. Wiley-Interscience, 2001.

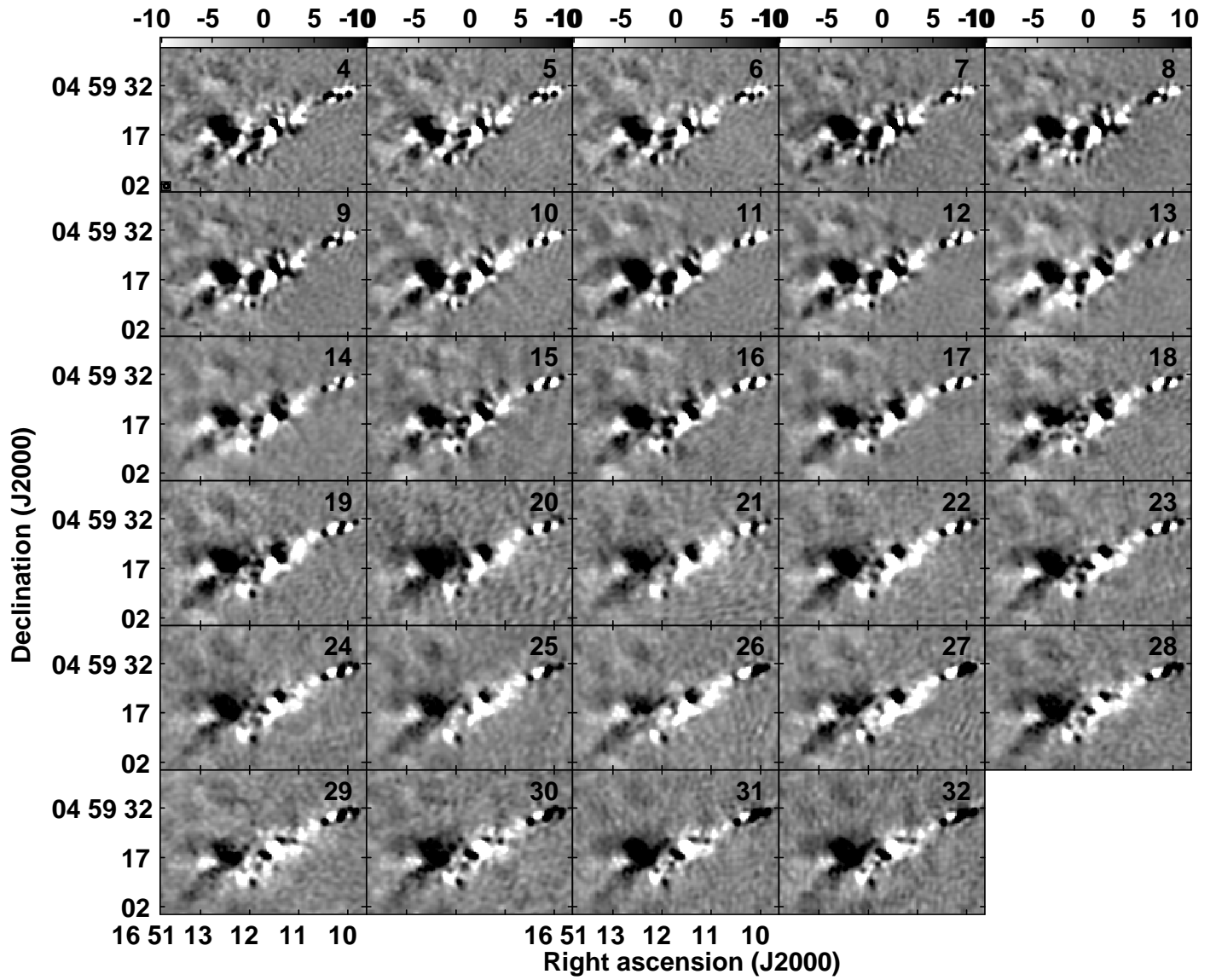


Fig. 11. Eastern jet and lobe of Her A in L band with 2% fractional bandwidth planes in Stokes Q. Resolution is 1.5" and the gray-scale bar at the top of each column is given in mJy bm^{-1} .

TABLE II
Instrumental Polarization Calibrators

3C286¹

Session	L		Clo		Chi		X	
	fpol(%)	R-L(°)	fpol(%)	R-L(°)	fpol(%)	R-L(°)	fpol(%)	R-L(°)
Ca	7.40	123						
Ba	8.78	70						
Bb	12.73	71						
Bc	5.27	55						
Aa	8.67	74						
Ab	7.25	63						
Af					11.4	68	10.7	52

J1504+1029

Session	L		Clo		Chi		X	
	fpol(%)	R-L(°)	fpol(%)	R-L(°)	fpol(%)	R-L(°)	fpol(%)	R-L(°)
Ca			2.93	77	2.70	73	2.33	67
Ba	2.20	103	2.83	36	2.56	31	2.34	14
Bb					2.73	22	2.89	23
Bc			2.26	25	2.56	37	2.37	42
Aa	2.77	78						
Ab	1.40	87						
Ac			2.73	29	1.99	19	1.19	23
Ad			2.66	26	1.71	18	1.13	23
Af			1.48	26	0.43	22	1.55	40

J1651+0129

Session	L		Clo		Chi		X	
	fpol(%)	R-L(°)	fpol(%)	R-L(°)	fpol(%)	R-L(°)	fpol(%)	R-L(°)
Da			5.72	-131	1.72	-159	1.49	104
Ca			2.88	-174	3.06	-174	3.30	-154
Ba			2.90	-150	3.05	-147	3.31	-154
Bb					2.84	-159	2.83	-143
Bc			3.30	-129	1.71	172	2.21	-156
Ac			3.01	-134	3.54	-131	3.45	-141
Ad			3.11	-141	3.24	-145	3.17	-147

¹ The R-L phase for 3C286 was set to 66°.

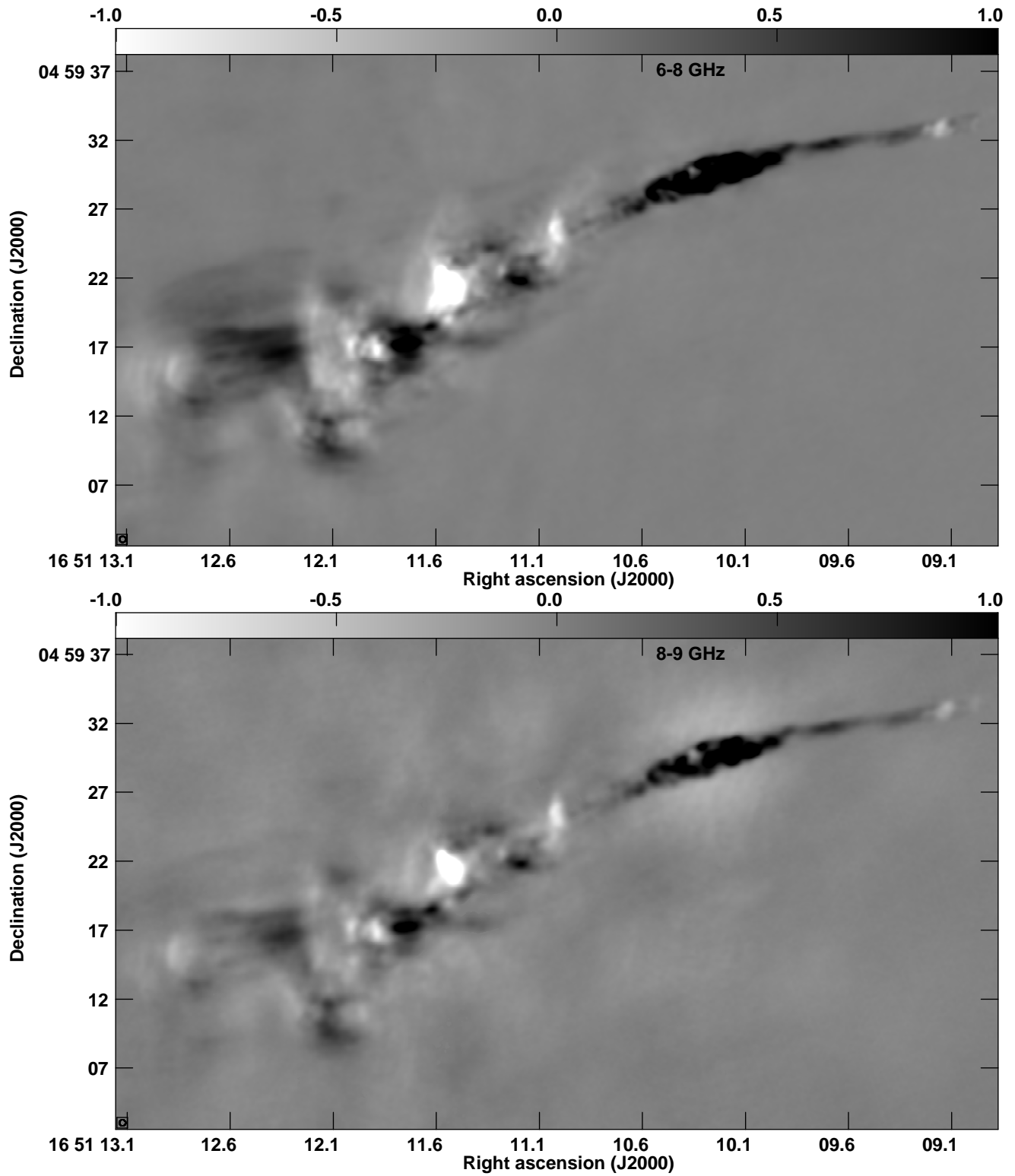


Fig. 12. Negative gray-scale of eastern jet and lobe of Herc A in Stokes Q. Resolution is $0.45''$ and the gray-scale bar at the top is given in mJy bm^{-1} . Above is Chi band (6–8 GHz) and below X band (8–9 GHz). Calibration artifacts are visible in the X band image, especially near the brightest portion of the jet.

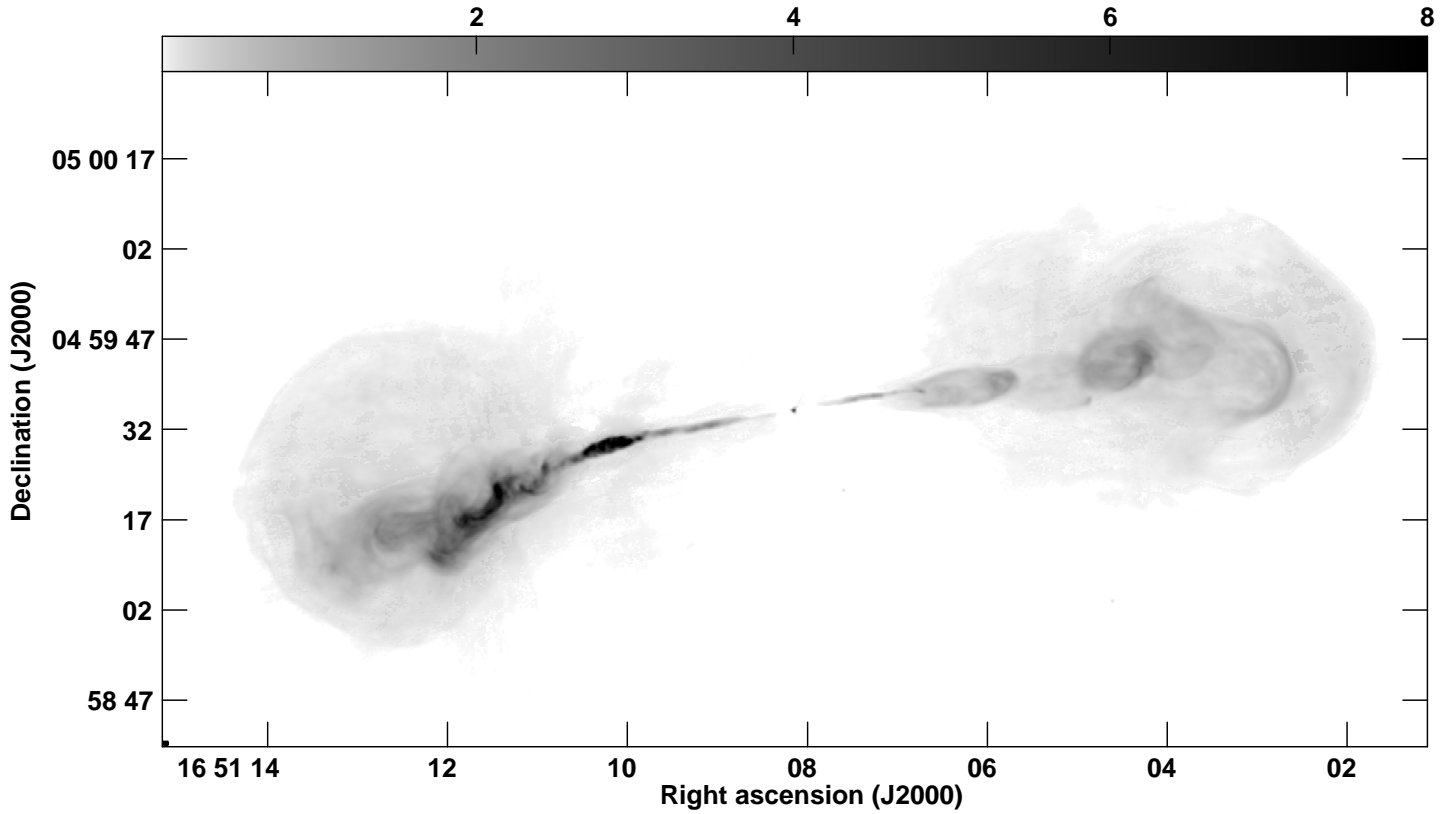


Fig. 14. Hercules A high resolution (0.45'') combined 4-9 GHz Stokes I image; gray scale labeled on top in mJy/bm.

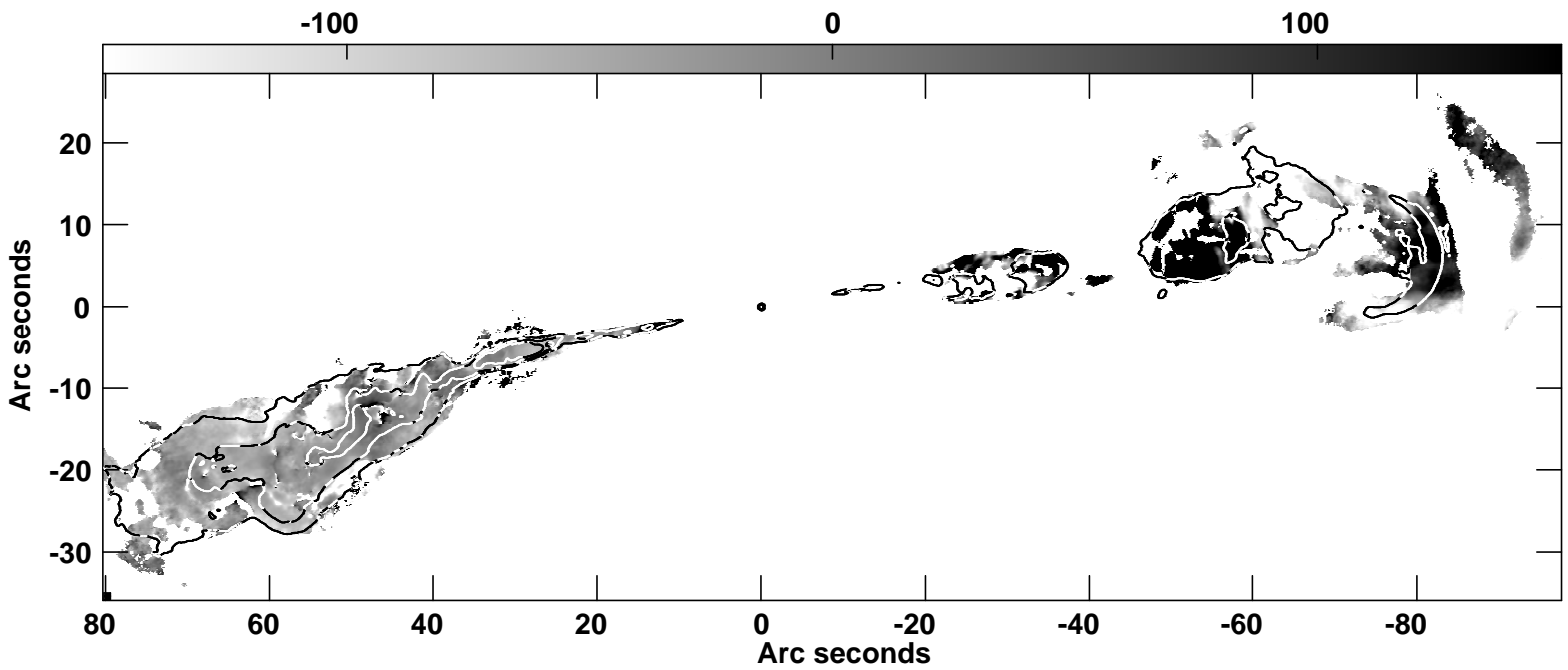


Fig. 15. Hercules A high resolution (0.45'') combined 4-9 GHz images. Rotation measure in gray-scale with scale bar at top in rad/m^2 ; Stokes I in contours at -0.1, 0.1, 0.3, 1 and 3 mJy/bm.